Satellite-based radar interferometry for monitoring ground surface deformation of filtered tailings storage facilities in continuous permafrost regions

Malte Vöge, Sean Salazar, & Regula Frauenfelder
Norwegian Geotechnical Institute, Oslo, Norway
Vincent Boulanger-Martel & Mutaz Nujaim
Research Institute on Mines and Environment, Université du Québec en Abitibi-Témiscamingue, Rouyn-Noranda, QC, Canada
Thomas Pabst
Department of Civil, Geological, and Mining Engineering, Polytechnique Montréal, Montréal, QC, Canada

ABSTRACT
An analysis of the possible ground deformation is necessary to properly design engineered covers for the reclamation of tailings storage facilities. This study uses satellite-based radar interferometry (InSAR) to map ground surface displacement rates at the Raglan Mine tailings storage facility. Persistent Scatterer (PS) and Small BAseline Subset (SBAS) analyses were performed to obtain a good coverage of the TSF and make coherent measurements across the seasons. Results indicate that the mean velocities obtained from the PS and SBAS analyses were below 5 mm/year. The optimal SBAS InSAR processing workflow yielded mean velocities of 4.44, 1.91, and -0.59 mm/year for the surface, east-facing slope, and south-facing slope of the tailings storage facility, respectively.

RÉSUMÉ
Une analyse des déformations possibles de la surface du sol est nécessaire pour concevoir adéquatement les recouvrements miniers construits sur les parcs à résidus. Cette étude vise à cartographier les taux de déplacement mesurés à la surface du parc à résidus minier filtrés de la mine Raglan. Cette étude a été réalisée en utilisant l'interférométrie radar par satellite (InSAR). Des analyses de diffuseurs persistants (PS) et de petits sous-ensembles de lignes de base (SBAS) ont été réalisées pour obtenir une bonne couverture du parc à résidus et effectuer des mesures cohérentes au fil des saisons. Les résultats indiquent que les vitesses moyennes obtenues à partir des analyses PS et SBAS étaient inférieures à 5 mm/an et, par conséquent, généralement faibles. La méthode d'interprétation SBAS optimale des données InSAR a donné des vitesses moyennes de 4,44, 1,91 et -0,59 mm/an pour le sommet, la pente est et la pente sud du parc à résidus, respectivement.

1 INTRODUCTION

There are an increasing number of mining projects being developed in Canada's Arctic regions where continuous permafrost is common. With the development of such mining projects, numerous unique engineering, environmental, and social acceptability challenges follow.

The environmental impacts of mining operations can be significant, especially when large volumes of tailings must be stored at the surface. The reclamation of tailings storage facilities (TSFs) frequently involves the use of engineered covers to control the generation and dispersal of contaminants in the environment. These cover systems are designed to be efficient for an indefinite time and, therefore, should require minimal long-term monitoring and maintenance. In this context, an analysis of the ground conditions and possible ground deformation is necessary to design cover systems accordingly. Significant ground surface movement could affect the performance of the cover system.

The geotechnical behavior of TSFs and tailings dams is usually monitored through classical geotechnical instrumentation and surveys. However, technical and logistical constraints, such as limited measurement density and frequency as well as difficulty accessing mine sites, make remote sensing tools a promising alternative for assessing ground surface deformation (e.g., Lato 2020; Scaioni et al. 2018; Stark et al. 2021).

A variety of satellite-based remote sensing technologies have successfully been used to monitor ground surface deformations of tailings dams and TSFs (e.g., Maltese et al. 2021; Stark et al. 2021). Notably, such deformations can be effectively monitored over wide areas with a millimetric precision using the synthetic aperture radar (SAR) interferometry (InSAR) technique (e.g., Grenerczy and Wegmüller, 2011; Du et al. 2020; Gama et al. 2020; Grebby et al. 2021). Differential interferometric SAR, or DInSAR, is a class of advanced, multi-temporal microwave remote sensing techniques that are used to determine surface deformations in the line-of-sight direction of a sensor by pairing SAR images of the same area acquired at different points in time (e.g., Iannacone et al. 2018; Stark et al. 2021). There are several unique algorithms that fall under the DInSAR umbrella, each with certain advantages and disadvantages depending on the application. The most widely used are the Persistent Scatterer (PS) and Small BAseline Subset (SBAS) approaches, which can provide a comprehensive view of

the behavior of a structure on a weekly or bi-weekly basis. Satellite-based InSAR can also provide an advantage through data archives that enable analyses to go back in time.

Filtered tailings are gaining popularity within the mining industry, particularly at mine sites operated in continuous permafrost regions. Filtered tailings are characterized by their higher percentage of solids (> 80-85%) as compared to conventional pulp (25-40% solids) and thickened (50-70% solids) tailings (Bussière 2007). Despite improved overall geotechnical properties (compared to conventional and thickened tailings), filtered TSFs can still display ground surface deformation over time. This study aims to map vertical displacement rates at the ground surface of the Raglan Mine filtered TSF (Katinniq, QC, Canada) using InSAR. Because snow-free seasons are short in continuous permafrost environments, specifically tailored InSAR processing workflows were developed to assess ground surface deformation in the TSF.

2 BACKGROUND – RAGLAN MINE

Raglan Mine (61°N; 73°W), which began operations in 1997, is a Ni-Cu-Co mine located on the Ungava Peninsula of Quebec. The mine sits between the Inuit communities of Salluit and Kangiqsujuak. At the site, the climatic conditions are sub-arctic, with a mean annual air temperature of -10.3 °C and total annual precipitation of about 560 mm.

Tailings produced at Raglan Mine's concentrator facility are filtered, then delivered by truck to a nearby TSF that was constructed at the onset of the mine's operations. The tailings are deposited in thin, compacted layers to ensure a good compaction and promote rapid freezing of the wastes. The Raglan TSF is approximately 35 m high, 750 m long and 600 m wide with a top surface sloped at 2% and sides sloped at 5:1.

Several studies have been carried out at the Raglan Mine to characterize the thermal and hydrogeological behavior of the filtered TSF and to develop reclamation solutions (Larochelle et al. 2021). Current closure plans involve reclaiming the TSF with a low saturated hydraulic conductivity cover system equipped with a geomembrane. Thus, a detailed analysis of the magnitude of actual and anticipated ground surface deformations is important to the cover design process and to ensuring the cover's long-term performance.

In 2012, a field-based investigation program was initiated to map and monitor ground surface deformations on Raglan mine's TSF (SNC-Lavalin, 2013). As a part of this program, four refrigerated boreholes were drilled in the TSF to retrieve intact, frozen filtered tailings cores. These cores were used to determine the tailings' in situ properties. For example, bulk density ranged from 1.95 to 2.35 g/cm^3; ice lenses ranged from 1 to 80 mm in thickness; and the water content of the tailings, which varied from borehole to borehole, ranged from 13% to 29%. These results suggested that the Raglan Mine TSF is stratified and composed of layers with variable properties in terms of compaction and ice content. However, this study was neither able to clearly determine the magnitude of ground surface deformations nor predict the magnitude of these deformations in the long term. The present study advances the current understanding of the geotechnical behavior of Raglan Mine's TSF by assessing short-term ground surface deformations using InSAR.

3 MATERIALS AND METHODS

3.1 Processing approach

In the present study, both PS and SBAS InSAR analyses were performed to assess the evolution of ground surface deformations at the Raglan mine the processing of SAR images was performed using ENVI SARscape® (L3Harris Geospatial / SARmap).

The PS technique was first proposed by Ferretti et al. (2001) and is based on identifying stable reflectors in multi-temporal interferometric SAR scenes. These stable reflectors (i.e., permanent or persistent scatterers) can be natural or man-made objects that present a stable signal phase from one acquisition to another, and thus display a high coherence over a SAR data stack. PS-InSAR uses these objects to deduce millimeter-scale deformations and obtain improved sub-meter digital elevation model accuracies. Ferretti et al. (2001) proposed an amplitude dispersion index for identifying PS candidates. A large data stack with a minimum of 25 acquisitions is necessary for this index to reliably identify persistent scatterers.

A single master image is selected and interferograms between this master and every other acquisition in the data stack are calculated. Although this approach includes interferograms with rather large temporal baselines, spanning up to several years, the persistent scatterers still provide coherent phase information due to their stable backscatter.

For the SBAS method (Berardino et al. 2002), a suitable combination of multiple interferograms, with corresponding small baselines, are implemented in a linear model. The SBAS method uses multi-looked data (downsampled to achieve square pixels) and applies spatial filtering before unwrapping the differential phase images. Therefore, the SBAS method is most suitable for natural terrains with a distributed scattering behavior.

For both processing methods, coherence is an important factor and only candidates/pixels with a coherence above a specified threshold are included in the result. The PS method only considers the temporal coherence since it operates on full resolution data and does not apply spatial filtering. The SBAS method considers both temporal and spatial coherence.

3.2 Data availability, coverage, and selected digital elevation model

The European Commission's Sentinel-1 mission is a two-satellite constellation (1A, 1B) that provides C-band wavelength SAR data with global coverage. Sentinel-1A was launched by the European Space Agency in April 2014, followed by Sentinel-1B in April 2016, which provided complementary data until a technical anomaly interrupted service in December 2021 (Sentinel-1C is scheduled to launch in 2023 to provide data continuity). The near-polar,

sun-synchronous Sentinel-1 constellation acquires data with at least a 12-day exact repeat cycle. The data are acquired either in ascending or descending orbit geometries, day or night, and in all weather conditions. The interferometric wide (IW) swath acquisition mode combines a swath width of 250 km with a medium spatial resolution of approximately 5 m in range by 20 m in azimuth. The analyses-ready Sentinel-1 data were obtained for free through the Copernicus Program.

First scenes for the target area were acquired in May 2015 and regular acquisition started in October 2016. The area is covered by two overlapping orbit tracks (Track 62 and Track 91; Figure 1). Due to the right-looking geometry of the sensor, the Raglan Mine tailings storage facility is located at far range for Track 62 and at near range for Track 91. Consequently, the incidence angle for the area of interest is smaller for Track 91 (i.e., the sensing vector is more vertical). This is an advantage, especially for measuring displacements at the slopes pointing away from the sensor (i.e., the northeast and southeast slopes; Figure 2). Therefore, Track 91 was selected for this study.

Figure 1: Radar image footprints of the Sentinel-1 interferometric wide swath mode acquisitions covering the Raglan TSF (yellow square) for Track 62 (blue) and Track 91 (red). Map source: Alaska Satellite Facility.

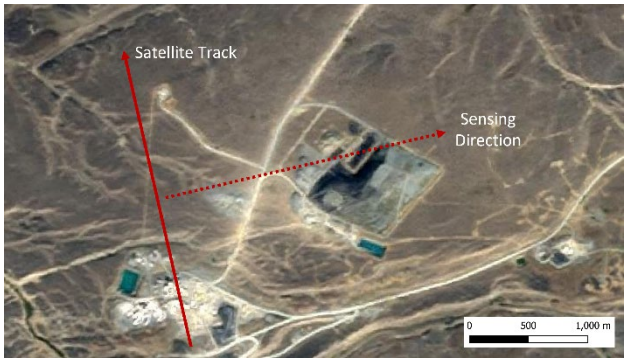

Figure 2: Orientation of the ascending orbit look direction over the TSF. (Map source: Google Earth).

At the time of analysis, 132 acquisitions were available for Track 91, of which only 44 acquisitions were taken during snow-free seasons (between June and September; Table 1) and useful for analysis. During image processing, a further seven images were excluded from the final analysis due to the presence of snow cover (in red; Table 1).

Table 1. Dates of Sentinel-1 SAR image acquisitions for Track 91 during the snow-free seasons between September 2016 and October 2020. Acquisitions in red were excluded due to the presence of snow cover.

Nr.	Date	Nr.	Date
1	16.08.2016	23	26.09.2018
2	03.06.2017	24	05.06.2019
3	15.06.2017	25	17.06.2019
4	27.06.2017	26	29.06.2019
5	09.07.2017	27	11.07.2019
6	21.07.2017	28	23.07.2019
7	02.08.2017	29	04.08.2019
8	14.08.2017	30	16.08.2019
9	26.08.2017	31	28.08.2019
10	07.09.2017	32	09.09.2019
11	19.09.2017	33	21.09.2019
12	01.10.2017	34	03.10.2019
13	29.05.2018	35	30.05.2020
14	10.06.2018	36	11.06.2020
15	22.06.2018	37	23.06.2020
16	04.07.2018	38	05.07.2020
17	16.07.2018	39	17.07.2020
18	28.07.2018	40	10.08.2020
19	09.08.2018	41	22.08.2020
20	21.08.2018	42	03.09.2020
21	02.09.2018	43	15.09.2020
22	14.09.2018	44	27.09.2020

3.3 SBAS processing

Given the general characteristics of the two aforementioned InSAR processing methods, the first choice for InSAR processing at Raglan was the SBAS method, as it is better suited for natural or smooth terrains.

A first SBAS analysis was done using, a maximum temporal baseline threshold of 60 days and a maximum perpendicular/spatial baseline of 3% (with respect to the critical baseline at which coherence becomes zero). To limit the total number of interferograms, the redundancy parameters were set to result in a connection graph with an average of about six interferograms per acquisition. Because of the long snow-covered seasons, the connection graph was allowed to be not fully connected. The resulting connection graph, shown in Figure 3, contains 101 pairs.

The greatest challenge for conducting InSAR measurements at Raglan Mine is the long snow-covered seasons, which are clearly visible in the connection graphs.

Snow cover in the area begins as early as late September and lasts until early June. Despite the revisit cycle of 12 days for Sentinel-1 at Raglan, the number of usable images per summer season is relatively low (about 7–10). This resulted in data gaps from late September to early June.

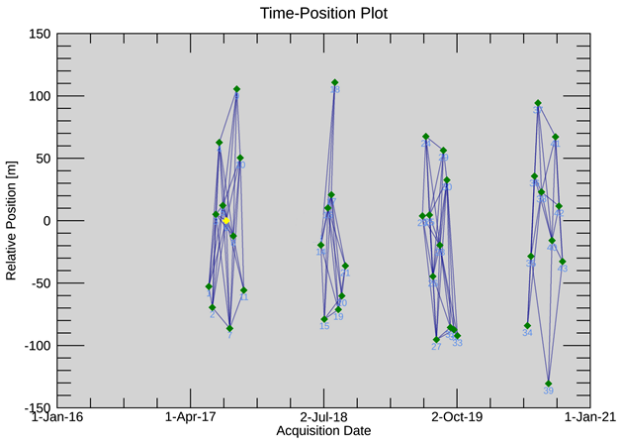

Figure 3: Connection graphs for the SBAS analysis with a 60-day temporal baseline threshold.

Because the connection graphs are not fully connected with the 60-day temporal baseline SBAS processing approach, another SBAS analysis was carried out, this time with a 320-day temporal baseline threshold. This resulted in a fully connected graph with connections across snow-covered seasons. The total number of interferograms was limited by the redundancy parameter and the resulting graph had an average of about six interferograms per acquisition. The resulting connection graph contains 118 pairs (Figure 4). For this processing method, two additional scenes were removed compared to the 60-day temporal baseline SBAS processing approach.

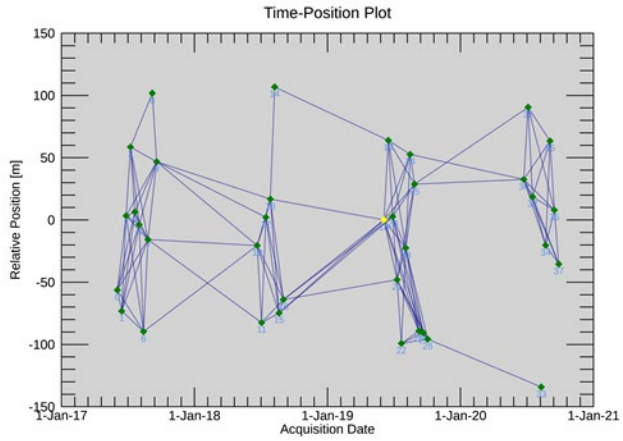

Figure 4: Connection graphs for the SBAS analysis with a 320-day temporal baseline threshold.

3.4 Persistent Scatterer processing

The same dataset was also analyzed with the PS processing workflow. Instead of pairing acquisitions according to their temporal baselines, the PS workflow selects one common reference acquisition and pairs all other acquisitions with the reference. This results in a star-shaped connection-graph (Figure 5).

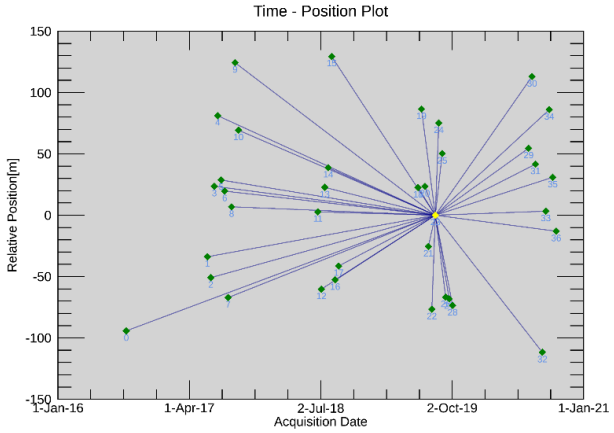

Figure 5: Connection graph for PS processing.

4 RESULTS

The different InSAR processing methods were compared in terms of their: (1) coverage of the TSF with coherent measurement points; (2) sensitivity to long data gaps introduced due to winter seasons; and (3) accuracy in terms of measured displacement rates.

4.1 SBAS processing – 60-day temporal baseline

Figure 6 depicts the mean velocity for the entire study area covered by the SBAS analysis for all points with a coherence value above 0.1. The colour-coded points represent the mean velocity in the line-of-sight of the radar beam, which is about 32° from the vertical (nadir). The colour code ranges from blue, representing uplift of 15 mm/year, to grey (stable areas), to yellow (-15 mm/year subsidence) to red (-30 mm/year). The outline of the TSF is marked by the polygonal bounding box. The results show strong variations over the entire area. Outside the TSF the results indicated strong subsidence, while the TSF itself showed much less movement.

Figure 7 presents a more detailed map of the displacement velocities in the area close to the TSF. The results indicate a strong subsidence of the natural ground around the TSF. In contrast, the TSF shows only limited displacements. Because the natural ground surrounding the TSF is mainly composed of intact or fractured rock, such subsidence was not expected. The source of these high subsidence values was investigated further by analyzing time series (Figure 8) obtained for two points on the TSF (a and b; Figure 7) and one point on the natural ground (c; Figure 7). The selected time series were modeled with a linear displacement model representing the measured mean velocity value (Figure 8a, b and c). The time-series fit the linear model well. However, due to the large data gaps in the winter seasons, and the fact that the connection graph is not fully connected, (i.e., no interferograms span the winter seasons), the information

from the individual summer seasons are not connected to each other.

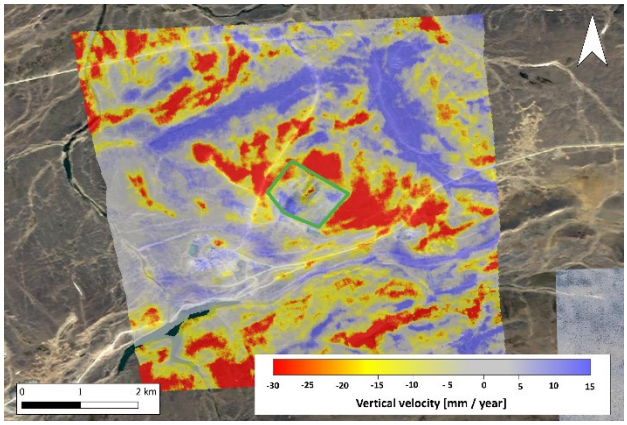

Figure 6: Mean velocity map for the 60-day temporal baseline SBAS processing approach.

Figure 8d presents an illustration of how the exact same data could be fitted to a displacement model following freeze and thaw cycles. Note that the snow-covered season is not visible in the measurements. A sinusoidal model can provide an equally good fit as compared to a linear model. However, the resulting mean velocity over the entire time series would in this case be close to zero, which is seen as much more reasonable for this area.

These results indicate that considering an incorrect model can result in a time series that provides a good fit, but still results in bad estimates of velocity. This is especially the case for the strong subsidence observed outside of the TSF at location c), which is most likely attributed to an incorrect fitting of the data to a linear model.

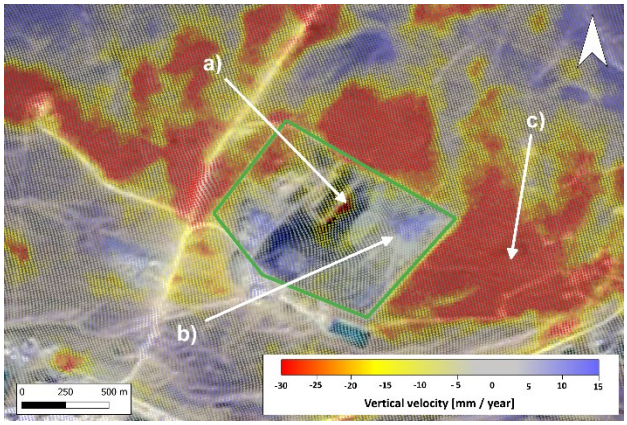

Figure 7: Detailed map of the mean velocity from the 60-day temporal baseline SBAS processing approach.

4.2 Persistent Scatterer processing

Figure 9 shows the velocity map generated using PS processing; all points have a coherence value ≥ 0.65. Note that the coherence values resulting from the PS and the SBAS methods do not represent the same measure and are not directly comparable.

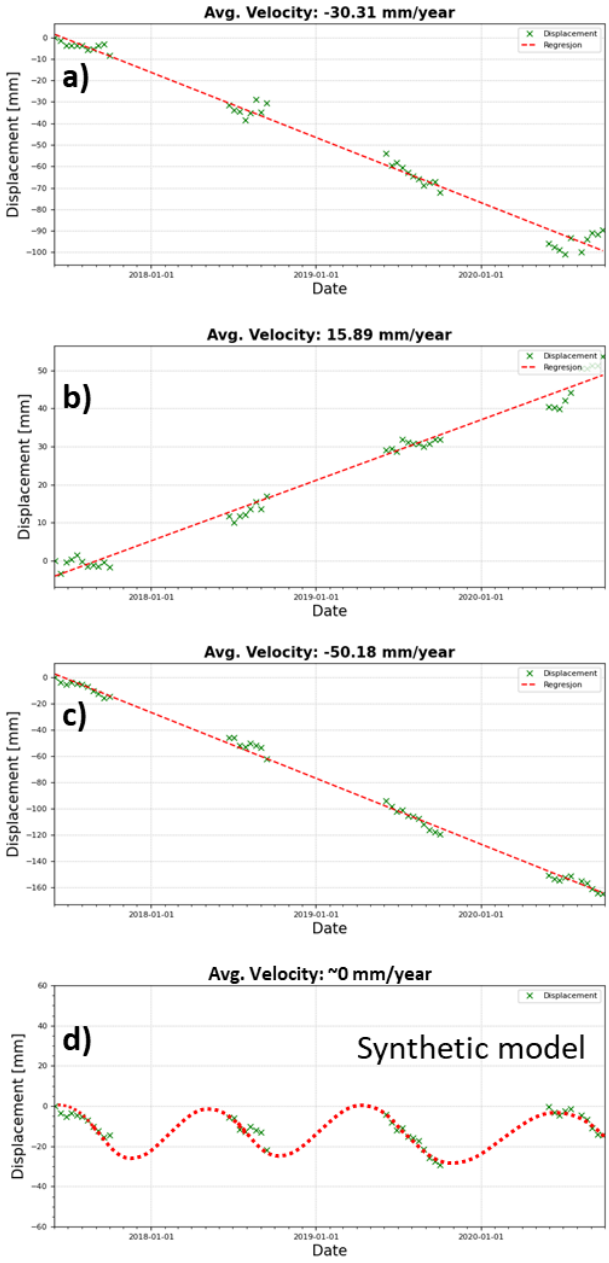

Figure 1: a), b), and c) Time series for points a, b, and c in Figure 7, respectively. Green crosses represent measured displacement values. Linear regression models shown as dashed red lines. d) shows the time series at point c manually fitted to an alternative displacement model with seasonal variations.

Figure 9 shows that there is no area of strong subsidence around the TSF, and the displacement results appear to be more stable over the area around the tailings. However, the PS processing approach yields poor coverage over the TSF despite a relatively low coherence threshold. This can be explained by the TSF's smooth surface, which lacks any conspicuous features that can provide a sufficiently stable signal backscatter. Because of the low coherence threshold, the results also include noise.

This is exhibited as the blue and orange points that are scattered across most of the study area. Figure 10 shows time series plots for points a) and b). Although there are still some indications of heave and subsidence across the monitoring seasons, the fully connected graph of the PS workflow allows for the use of a linear regression model. Overall, the mean velocities are close to 0 for most of the surface.

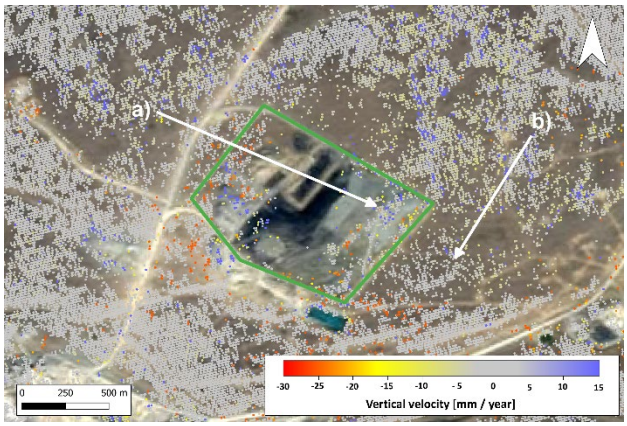

Figure 9: Mean velocity map for PS analysis. The white arrows mark measurement points for the time series shown in Figure 10.

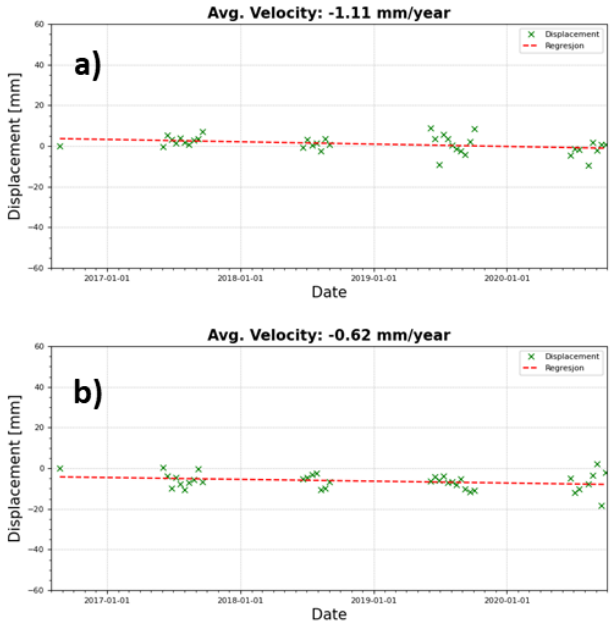

Figure 10: a) and b) Time series for points a and b in Figure 9, respectively. Green crosses represent measured displacement values. Regression models are shown as dashed red lines and represent the mean velocities.

4.3 SBAS processing – 320-day temporal baseline

For the 320-day temporal baseline SBAS processing approach, the winter seasons are spanned with 4–7 pairs each. This provides some redundancy for connecting the measurements of the different seasons. Figure 11 presents the mean velocity map obtained for this processing approach for all measurement points that had a coherence above 0.1. Similar to the PS analyses, the strong variations that were observed in the 60-day temporal baseline SBAS processing approach are no longer visible. In light of these results, it can be concluded that the interferometric pairs spanning the snow-covered seasons resolved issues associated with fitting linear models.

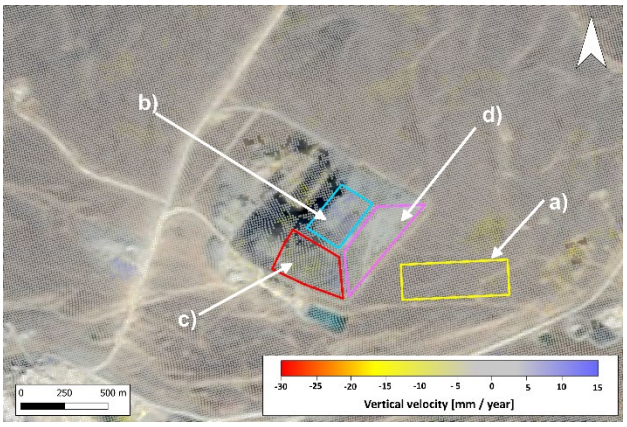

Figure 11: Mean velocity map for the 320-day temporal baseline SBAS processing approach. Colored polygons a), b), c), and d) mark the areas for which averaged time series are shown in Figure 12.

The 320-day temporal baseline SBAS processing approach still provides good spatial coverage of the TSF. Measurements over the TSF are considerably denser than for the PS approach. This was expected because the TSF has a smooth surface (character of distributed scattering) that lacks the persistent scatterers required for the PS method. The eastern part of the TSF is entirely covered with measurement points. However, there are some areas without measurement points in the western portion of the TSF. This is likely related to tailings deposition activities at the site that occurred during the measurement period. Results in this area should be considered with special care, as measurements could still be affected by mass movements, even if their average temporal coherence lies above the threshold of 0.1.

Figure 12 presents time series for the four areas outlined in Figure 11. The time series for the area outside the TSF (Figure 12a) indicates, that the linear model properly handles seasonal variations. The resulting mean velocity (averaged over the area) is only -0.59 mm/year which can be regarded as negligible. Figure 12b, c, and d show the time series obtained for the TSF surface, south slope, and east slope, respectively. The results generally indicated low displacement velocities. The surface of the TSF showed some indication of upward movement, with a mean velocity of 4.44 mm/year averaged over the area. The east-facing slope showed a slight upward-movement of 1.91 mm/year. The south-facing slope showed some patches with downward movement, however, the mean velocity was only -0.59 mm/year on average. No large displacement patterns were visible over the entire tailings.

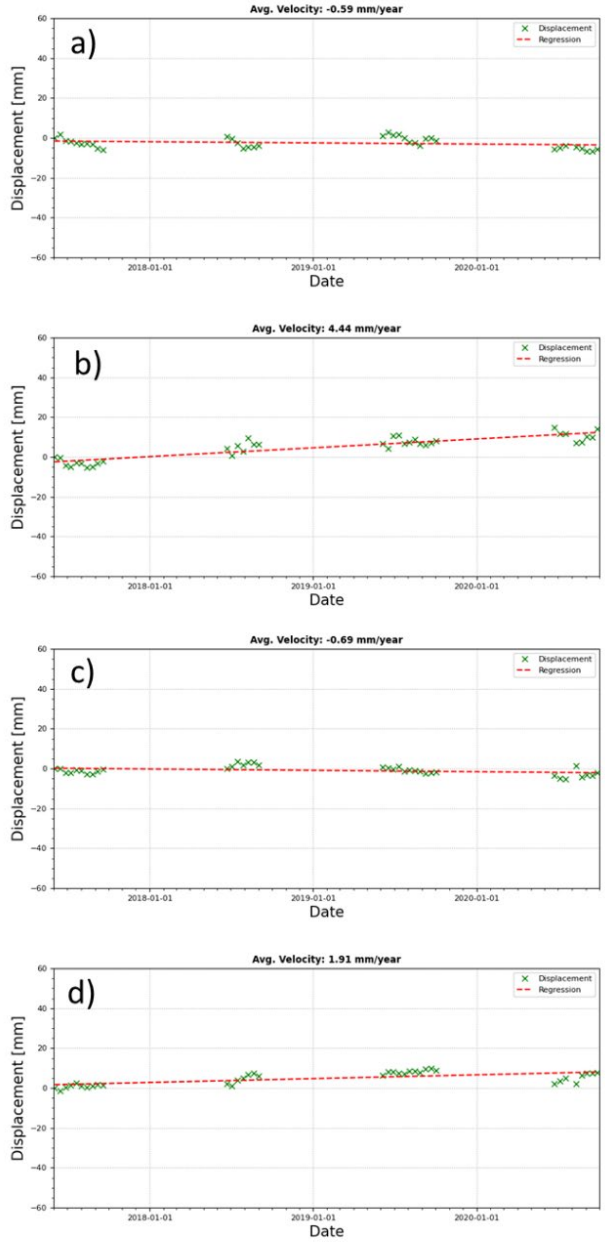

Figure 12: Averaged time series for SBAS processing (320-day temporal baseline) of the areas marked in Figure 11. Mean time series for a selected area close to the TSF (a) and mean time series for the top (b) as well as the South (c) and East (d) slopes.

4.4 Measurement accuracy

To estimate the accuracy of the measurements provided by each of the processing approaches, an area northwest of the TSF was selected for analysis (Figure 13). The overall mean velocity and the standard deviation of the velocity were calculated for this area using each of the tested processing methods (Table 2). Because this area is mainly composed of intact or fractured rock, it is expected to be stable in terms of ground movement over a year (i.e., mean velocity ≈ 0 mm/year). Therefore, both, the mean velocity and standard deviation should be close to zero in this area. A mean velocity outside the range of ± 2–3 mm/year indicates a general bias or offset in the measurements. A standard deviation of above 3 mm/year indicates an increased amount of noise.

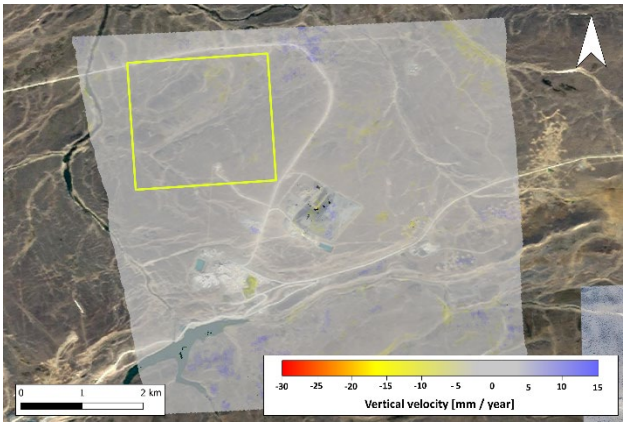

Figure 13: Area used to evaluate the accuracy of the three processing methods. The measurements of the 320-day temporal baseline SBAS processing approach are shown for spatial reference.

Table 1. Statistical measures for the test-area.

	60-day SBAS	PS	320-day SBAS
Number of points	18951	30920	25266
Mean Velocity [mm/year]	-6.18	-0.64	-0.17
Std.-Dev. Velocity [mm/year]	17.54	3.38	1.31

Both the mean velocity and standard deviation of the 60-day temporal baseline SBAS approach were high. This is consistent with the results and observations discussed in Section 4.2. The mean velocity for both the PS and the 320-day temporal baseline SBAS processing approach show much lower mean velocity values, as they were able to track and correctly fit the seasonal variations to linear displacement models. With a standard deviation of ± 3.38 mm/year, the PS approach showed a higher degree of noise, which is also consistent with the observations discussed in Section 4.3. The 320-day temporal baseline SBAS approach provided the highest accuracy. Given that long snow-covered seasons severely limited the number of acquisitions at the study site, a precision of 1.3 mm/year can be considered very good.

5 CONCLUSION

Mapping of displacements at the Raglan Mine TSF was successfully carried out using InSAR. As expected, the

long snow-covered seasons presented the biggest challenge since they resulted in large data gaps that made consistent measurements across seasons difficult. SBAS processing with a 60-day temporal baseline showed how these data gaps can affect the reliability of InSAR analyses. The PS processing approach solved the problem of the long data gaps. However, the results were noisy and only a very small number of measurement points could be achieved over the TSF. SBAS processing was repeated with a 320-day temporal baseline, which resulted in more consistent measurements across seasons and good coverage over the TSF. By increasing the temporal baseline threshold to 320 days, acquisition pairs were able to be connected across the snow-covered seasons.

The TSF surface and the east-facing slope showed slight indications of upward movement, while the south-facing slope showed slight downward movement. However, the measured displacement velocities in the TSF were generally small. In both SBAS approaches, displacements were averaged over 15 m x 15 m resolution cells and additional spatial filtering was applied. Therefore, greater displacements over small spatial extents may have appeared smaller in magnitude, but larger in spatial extent. This means that, depending on the magnitude, some smaller but significant (to the cover design) differential settlement may have been ignored by the developed monitoring approach.

The present study is part of a larger study that aims to assess ground deformations at the Raglan Mine TSF. Additional monitoring via field investigations and remote sensing will be conducted to establish the current state of the TSF's deformations, especially with respect to differential settlements.

6 ACKNOWLEDGMENTS

This study was funded by the *Fonds de recherche du Québec – Nature et technologies* (FRQNT) as a part of the *Développement durable du secteur minier* program and by the Research Institute on Mines and the Environment (http://www.irme.ca). This study was also supported by NGI's internal project "SP12 – Sustainable Mine Tailings". The authors wish to thank the staff of Raglan Mine's environment department for their collaboration.

7 REFERENCES

Berardino, P., Fornaro, G., Lanari, R. and Sansosti, E. 2002. *A new algorithm for surface deformation monitoring based on small baseline differential SAR interferograms*. IEEE Transactions on Geoscience and Remote Sensing, 40(11), 2375–2383.

Boulanger-Martel, V. 2019. Évaluation de la performance de recouvrements miniers pour contrôler le drainage minier acide en climat arctique. PhD diss., Polytechnique Montréal.

Bussière, B. (2007). Colloquium 2004: Hydrogeotechnical properties of hard rock tailings from metal mines and emerging geoenvironmental disposal approaches. Canadian Geotechnical Journal, 44(9), 1019-1052.

Du, Z., Ge, L., Ng., A., Zhu, Q., Horgan, F. and Zhang, Q. (2020). Risk assessment for tailings dams in Brumadinho of Brazil using InSAR time series approach. Science of the Total Environment. 717.

Ferretti, A., Prati, C. and Rocca, F. 2001. Permanent Scatterers in SAR Interferometry. IEEE Transactions on Geosciences and Remote Sensing, 39(1), 8–20.

Gama, F.F., Mura, J.C., Paradella, W.R. and de Oliveira, C.G. (2020). Deformations Prior to the Brumadinho Dam Collapse Revealed by Sentinel-1 InSAR Data Using SBAS and PSI Techniques. Remote Sensing, 12(3664).

Grebby, S., Sowter, A., Gluyas, J., Toll, D., Gee, D., Athab, A. and Girindran, R. (2021). Advanced analysis of satellite data reveals ground deformation precursors to the Brumadinho Tailings Dam collapse. Communications Earth & Environment, 2(1), 1-9.

Grenerczy, G. and Wegmüller, U. (2011). Persistent Scatterer Interferometry analysis of the embankment failure of a red mud reservoir using ENVISAT ASAR data. Nat.Hazards 59,1047–1053.

Iannacone, J. P., Lato, M., Troncoso, J. and Perissin, D. (2018). InSAR monitoring of active, inactive and abandoned tailings facilities. In Proceedings of the 5th International Seminar on Tailings Management, Santiago, Chile (pp. 11-13).

Larochelle, C.G., Bussière, B., Boulanger-Martel, V., Wilson, W., and Rivest, É. In situ thermal behavior of an insulation cover for mine site reclamation in arctic climate. 74th Canadian Geotechnical Conference, Niagara, ON, Canada.

Lato, M. (2020). Canadian Geotechnical Colloquium: three-dimensional remote sensing, four-dimensional analysis and visualization in geotechnical engineering — state of the art and outlook. Canadian Geotechnical Journal, 58, 1065-1076.

Maltese, A., Pipitone, C., Dardanelli, G., Capodici, F. and Muller, J.P.. (2021). Toward a Comprehensive Dam Monitoring: On-Site and Remote-Retrieved Forcing Factors and Resulting Displacements (GNSS and PS–InSAR). Remote Sensing, 13(1543).

Massonnet, D. and Feigl, K. L. (1995). Satellite radar interferometric map of the coseismic deformation field of the M= 6.1 Eureka Valley, California earthquake of May 17, 1993. Geophysical Research Letters, 22(12), 1541-1544.

Massonnet, D. and Rabaute, T. (1993). Radar interferometry: limits and potential. IEEE Transactions on Geoscience and Remote Sensing, 31(2), 455-464.

Scaioni, M., Marsella, M., Crosetto, M., Tornatore, V. and Wang. (2018). Geodetic and Remote-Sensing Sensors for Dam Deformation Monitoring. Sensors, 18(3682).

SNC-Lavalin. (2013). Tailings storage facility deformation study. Final report.

Stark, T. D., Oommen, T., Ning, Z. (2021). Remote Sensing for Monitoring Embankments, Dams, and Slopes: Recent Advances. Geotechnical special publication n.322, American Society of Civil Engineers Reston, VA.